
Thermal Distortions in Laser-Diode– and Flash-Lamp–Pumped Nd:YLF Laser Rods

Laser-diode pumping of solid-state laser materials is proving to be much more advantageous over the more conventional technique of flash-lamp pumping. The electrical to optical efficiency of laser diodes is significantly higher than for flash lamps. In addition, the emission wavelength of laser diodes can be chosen to couple efficiently to the absorption band of the laser ion, resulting in very high overall laser efficiencies. Despite this level of efficiency, both laser-diode– and flash-lamp–pumped systems deposit unwanted heat into the gain medium. The resultant thermal loading of the gain medium leads to thermal-optical wavefront distortions that can degrade the performance of a laser system. Exact eigenmode solutions of optical resonators with phase-aberrating elements can be numerically calculated using high-speed computers. These calculations require a detailed knowledge of the wavefront distortions induced by optical pumping in order to design compensating optics for the system. This is especially important when designing a high-average-power laser system.

A practical constraint for large Nd:glass master oscillator power amplifier (MOPA) laser systems, such as those for laser fusion, is that the laser oscillator must be wavelength matched to the Nd:phosphate-glass amplifiers (gain peak at 1053 nm).¹ A convenient laser crystal with this property is Nd:YLF. A Nd:YLF crystal is naturally birefringent and exhibits gain at 1053 nm for radiation polarized with the electric field perpendicular to the crystalline c axis (σ -polarization state) and exhibits gain at 1047 nm for radiation polarized with the electric field parallel to the crystalline c axis (π -polarization state). This crystal has many other features that make it desirable for other applications, but these will not be elaborated on here.

Thermal-lensing measurements on a Nd:YLF laser rod were first performed by Murray² using pulsed excitation at a fixed input energy. The measurements were made by passing a beam through the rod followed by a lens and a movable pinhole (a standard technique for measuring isotropic crystals). Detailed measurements were later made by Vanherzeele^{3–5}

with a different technique showing strong thermal astigmatism as well as thermal lensing. Astigmatism was measured by using a slit (as opposed to a pinhole) oriented parallel and perpendicular to the crystal c axis. This gives two thermal-focal-length measurements for each polarization state (σ and π): one focal length for a narrow slit of rays oriented parallel to the crystal c axis and one for a narrow slit of rays oriented perpendicular to the crystal c axis. Vanherzeele shows how these thermal distortions, which can adversely affect the performance of a laser system, can be effectively eliminated by proper choice of compensating optics and by the use of a dual-laser-rod system. Further thermal-lensing measurements were made by Reed and Frangineas⁶ who give the rod thermal-focal lengths at a fixed input power both parallel and perpendicular to the c axis for σ - and π -polarization states. Later Cerullo *et al.*⁷ provided additional thermal-lensing data taken as a function of their krypton-flash-lamp electrical-pumping power. In the above experiments, krypton flash lamps were used as excitation sources for all measurements with the exception of the work by Murray, who used xenon flash lamps.

In this article we describe detailed interferometric measurements of the thermal distortions in two Nd:YLF laser rods. One rod is pumped with a xenon flash lamp and the other with laser diodes. Each rod is pumped to the same small-signal gain to compare its distortions under similar laser-operating conditions. We characterize these thermal distortions in terms of a set of primary aberrations of defocus, astigmatism, coma, and spherical. We show that defocus and astigmatism are the dominant aberrations. We interpret our interferometric measurements in terms of the conventional thermal-focal lengths parallel and perpendicular to the c axis of the crystal for both polarization states. We compare the thermal-focal lengths measured with our xenon-flash-lamp– and laser-diode–pumped rods when pumped to the same small-signal gain. We calculate effective dioptric-power coefficients from our data to compare to those reported in the literature for krypton-flash-lamp pumping. We also directly measure the thermal relaxation of these thermal distortions with time for our laser-diode–pumped rod.

We believe that our measurements comparing flash-lamp to laser-diode pumping, as well as our thermal relaxation measurements, are the first measurements of this kind.

Experimental Setup

To measure the thermal distortions in our flash-lamp- and laser-diode-pumped Nd:YLF laser rods, the rods were separately placed in one arm of a Mach-Zehnder interferometer as shown in Fig. 71.38. The laser source for the interferometer was a Nd:YLF cw-mode-locked laser operating at a 1053-nm wavelength (this laser was chosen for convenience). The detection system (CCD camera) integrated over many milliseconds and, hence, could not resolve individual pulses in the mode-locked pulse train. The path lengths of the two interferometer arms were carefully adjusted to be approximately equal in order to produce high-contrast fringes. Wedge was introduced in the interferometer by adjusting the mirrors to provide approximately 40 fringes of tilt. To analyze the fringes, the rod was imaged onto a CCD camera with a lens placed outside the interferometer. The images of the high-contrast fringes from the camera were digitized with a computer equipped with a frame-grabber board. The camera was spectrally filtered with appropriate blocking filters to pass only the 1053-nm radiation of the interferometer laser source. The gain at the 1053-nm wavelength provided by the rod being tested did not significantly degrade the fringe contrast. Fluorescence from the pumped rod was effectively blocked with an aperture placed in the rod arm of the interferometer approximately 50 cm from the rod. The aperture diameter was adjusted to limit the angular field of view of the camera-collection optics while not introducing additional aberrations. The laser used for the interferometer was linearly polarized, and the rod was placed between two half-wave plates (HWP). The laser rods were fabricated with the crystalline a axis along the length of the rod and were placed in the interferometer with the a axis parallel to the interferometer optical axis. The crystalline c axis for

both the laser-diode and flash-lamp systems was therefore perpendicular to the interferometer optical axis and located in the plane of the rod end face. The interferometer laser polarization through the rod could be adjusted perpendicular to the c axis (σ) or parallel to the c axis (π) of the rod by adjusting the half-wave plate before the rod. The half-wave plate after the rod was used to realign the laser polarization state parallel to the interferometer reference arm for maximum fringe contrast on the camera. Fringes were captured by the computer and analyzed.

The digitized fringe patterns were transformed into wavefronts using a spatial-synchronous phase-detection technique.⁸⁻¹⁰ The high-frequency interferogram was captured by the frame grabber, stored in memory, and then Fourier analyzed to obtain the amplitude and phase of the two-dimensional wavefront exiting the laser rod. Fringe data were analyzed over only a portion of the rod's clear aperture (approximately 90% of the rod diameter) to obtain the wavefront distortions. To accomplish this, a circular software aperture centered on the rod was placed over the rod image. Only the fringe data within this aperture were used in the analysis. To calibrate the fraction of the rod aperture used in the analysis, a reticle was placed at the equivalent rod position in the opposite interferometer arm, imaged to the camera with the lens outside the interferometer, and overlapped in software with the image of the rod and the software aperture used for fringe analysis. A background wavefront was taken for each rod with no pumping (but with the simmer on for the flash-lamp data) and subtracted from all other wavefronts. The background-subtracted wavefronts of the pumped rods were then analyzed to determine the number of waves of defocus, astigmatism, spherical, and coma produced by pumping. The overall accuracy of this fringe analysis technique is believed to be $<\lambda/50$ (<0.02 waves). To calibrate this interferometric-measurement system, the focal length of a 1-m lens was measured with an accuracy of greater than 99%.

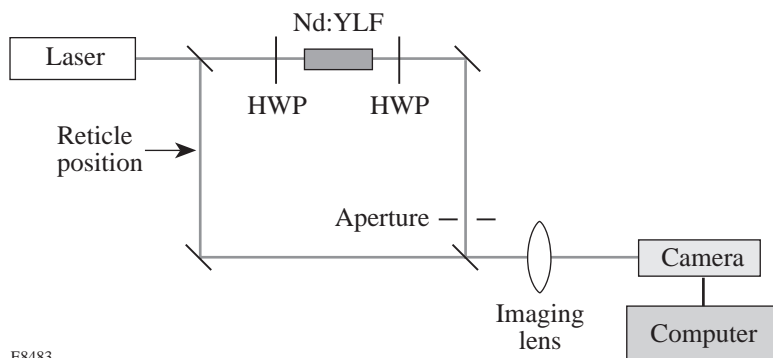


Figure 71.38
Experimental setup for measuring the pump-induced wavefront distortions in Nd:YLF laser rods.

E8483

The thermal-time constant of our laser-diode-pumped Nd:YLF rod was also measured with the above equipment. The fringes were recorded on tape with a video camera recorder (VCR) as the rod pumping was turned off (and the liquid cooling left on). A frame sequencer was used to number the individual frames from the camera. By replaying the video tape through the computer, sequential data frames could be captured and analyzed. In this way, the aberrations could be measured at 60 frames (data points) per second.

The flash-lamp system had a 4-mm-diam \times 54-mm-long Nd:YLF laser rod pumped with a single 4-mm bore \times 24-mm-arc-length xenon flash lamp. The flash lamp was simmered with approximately a 400-V drop across the lamp and 50 mA of simmer current. The pulse-forming network for the lamp used a 150- μ f capacitor charged to 385 V (i.e., 11 J per pulse). The lamp's current pulse was approximately Gaussian with a pulse width of 250 μ s (FWHM). A small-signal gain of 1.8 at 1053 nm was measured in the Nd:YLF rod with these conditions (sufficient to operate the regenerative amplifier for our application). The system was operated to 60 pulses per second. Fringes within a 3.4-mm-diam software aperture centered on the rod were used to analyze this rod.

The laser-diode-pumped system, including the diode arrays, was designed and built by the McDonnell-Douglas Electronic Systems Company (no longer a part of McDonnell-Douglas) and is similar in performance (although operating at a different wavelength) to the one reported in Ref. 11. The system had a 5-mm-diam \times 54-mm-long Nd:YLF laser rod pumped with three banks of laser diodes along the length of the rod. Each bank consisted of 16 diode bars arranged symmetrically around the circumference of the rod for a total of 48 diode bars arranged around the rod. The length of the rod pumped with this diode arrangement was 34 mm. The laser diodes had their polarization states parallel to the a axis of the crystal and hence perpendicular to the c axis. The diode emission wavelengths were centered around the 797-nm absorption peak of Nd:YLF. The absorption coefficient of Nd:YLF for this case is approximately 3 cm^{-1} . The pulse-forming network produced a 250- μ s-wide, 50-A square current pulse with approximately 100 V applied across the diode bars connected in series. With these conditions each diode bar emitted approximately 45 W of peak optical power (2.16-kW peak array optical power) for an optical-output-to-electrical-input diode-array efficiency of greater than 40%. A small-signal gain of 1.8 at 1053 nm was measured in the rod under these conditions. If we assume a stimulated emission cross section of $1.2 \times 10^{-19} \text{ cm}^2$ for this

transition,¹² the stored energy in the rod was 0.18 J, resulting in an optical-pumping efficiency (stored energy to diode-array output-optical energy) of approximately 33%. This system was operated to 200 pulses per second. Fringes within a 4.4-mm-diam software aperture centered on the rod were used to analyze this rod.

Interpretation of Interferometric Data

When the Nd:YLF laser rod is unpumped, the wavefront distortion measured in transmission through the rod by the interferometer gives the amount of static aberration in the rod due to internal crystal strain. This wavefront is stored and is the background wavefront that is subtracted from all other measured wavefronts. The background-subtracted wavefronts measured with optical pumping, therefore, provide detailed information of the thermally induced refractive-index changes in the pumped laser rods. The distorted wavefronts exiting the thermally loaded laser rods are quantified in lowest order (using the third-order aberration theory¹³) by the linear superposition of a set of primary aberrations of defocus, astigmatism, coma, and spherical, which are defined below.

The thermally distorted wavefront exiting the rod can be expressed as a surface of constant phase:

$$\Phi_{\text{total}}(\rho, \theta) = \Phi_{\text{def}}(\rho) + \Phi_{\text{ast}}(\rho, \theta) + \Phi_{\text{coma}}(\rho, \theta) + \Phi_{\text{sph}}(\rho), \quad (1)$$

where the surface of constant phase for each of the primary aberrations is given by

$$\Phi_{\text{def}} = \lambda \Delta_{\text{def}} \rho^2, \quad (2a)$$

$$\Phi_{\text{ast}} = -\frac{\lambda \Delta_{\text{ast}}}{2} \rho^2 \cos(2\theta), \quad (2b)$$

$$\Phi_{\text{coma}} = -\lambda \Delta_{\text{coma}} (\rho^3 - \rho) \cos(\theta), \quad (2c)$$

$$\Phi_{\text{sph}} = \lambda \Delta_{\text{sph}} (\rho^4 - \rho^2), \quad (2d)$$

with $\rho = r/r_0$ the normalized radius r within the rod aperture, r_0 is the radius of the rod clear aperture used in the analysis ($r_0 = 1.7 \text{ mm}$ for the flash-lamp-pumped rod and $r_0 = 2.2 \text{ mm}$ for the laser-diode-pumped rod), θ is the polar angle in the rod

aperture measured from the c axis of the crystal, λ is the interferometer wavelength (1053 nm), and the Δ_i 's are the number of waves of the primary aberration measured (i.e., the weighting factors in the linear superposition).

We show experimentally that the dominant thermal aberrations are defocus and astigmatism (discussed in the next section). Both defocus and astigmatism have a quadratic dependence on the aperture coordinate r , and from these a focal length can be defined for two orthogonal planes. If we neglect the aberrations of coma and spherical, then we can define a focal length for the two orthogonal planes that contain the a axis (optical axis) of the crystal. (The plane containing the a and c crystal axes with $\theta = 0$ is referred to as $\parallel c$, and the plane containing the a and b crystal axes with $\theta = \pi/2$ is referred to as $\perp c$.) The wave fronts (surfaces of constant phase) associated with defocus and astigmatism are shown in Fig. 71.39. Pure defocus [Fig. 71.39(a)] is seen to be a spherical wavefront with equal curvatures in all directions (i.e., $0 \leq \theta < 2\pi$). Pure astigmatism [Fig. 71.39(b)] is seen to be a wavefront with curvatures of equal magnitude but opposite sign in two orthogonal directions (i.e., $\theta = 0$ and $\theta = \pi/2$). The thermal-focal length in a given plane is easily calculated from the number of waves of defocus and astigmatism and is given by (using a small angle approximation)

$$f_{\pm} = \frac{r_0^2}{2\lambda(\Delta_{\text{def}} \pm \Delta_{\text{ast}}/2)}, \quad (3)$$

where f_+ is the focal length in the plane perpendicular to the crystal c axis ($\theta = \pi/2$ or $\perp c$) and f_- is the focal length in the plane parallel to the crystal c axis ($\theta = 0$ or $\parallel c$).

Astigmatism and coma are odd aberrations and have an angle of symmetry associated with them. The wavefront analysis program calculates this symmetry angle for these aberrations, and our measurements show that these symmetry axes are aligned perpendicular and parallel to the c axis of the crystal as implied by Eqs. (2)—an expected result but previously unmeasured. The definitions and conventions discussed here were used to analyze our data.

Thermal-Distortion Measurements

We assume that the laser-diode- and flash-lamp-pumped rods are uniformly pumped so that heat is generated uniformly throughout the rod volume. Since the time between pump pulses is short (0.2 s for the lowest pulse-repetition rate used: 5 Hz) compared to the thermal-relaxation time of the rod (1.5 s; see Fig. 71.45 discussed later), pumping can be considered continuous and the temperature distribution in the rod will reach steady state after a brief warm-up period. The rods were liquid cooled, and in steady state the surface temperature of the rod will be constant for a particular pump power. A long cylindrical laser rod pumped with the above assumptions will produce a quadratic radial temperature and strain distribution that will lead to a quadratic radial index-of-refraction profile in the rod.¹² Since Nd:YLF is a uniaxial crystal, the quadratic radial profile will be different in two orthogonal directions.

Figure 71.40 shows the measured aberrations as a function of the pump repetition rate for the case of the laser-diode-pumped laser rod using π -polarized light in the rod (gain at $\lambda = 1047$ nm). Figure 71.41 shows the same measurements using σ -polarized light in the rod (gain at $\lambda = 1053$ nm). In these figures, the data points for defocus and astigmatism are fit to a straight line, while the data points for coma and spherical are

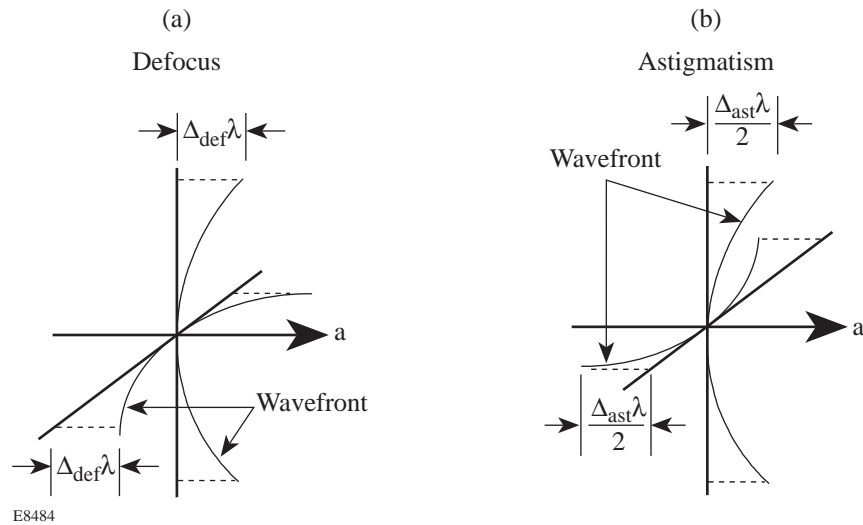
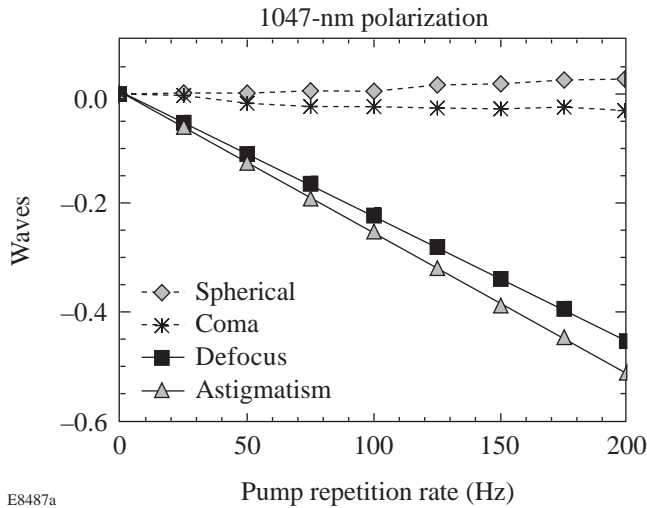


Figure 71.39
Surfaces of constant phase (wavefront shown with thin lines) for (a) pure defocus and (b) pure astigmatism as defined and used in our analysis. Here λ is the wavelength of the interferometer source (1053 nm), Δ_{def} is the number of waves of defocus measured, and Δ_{ast} is the number of waves of astigmatism measured.

E8484

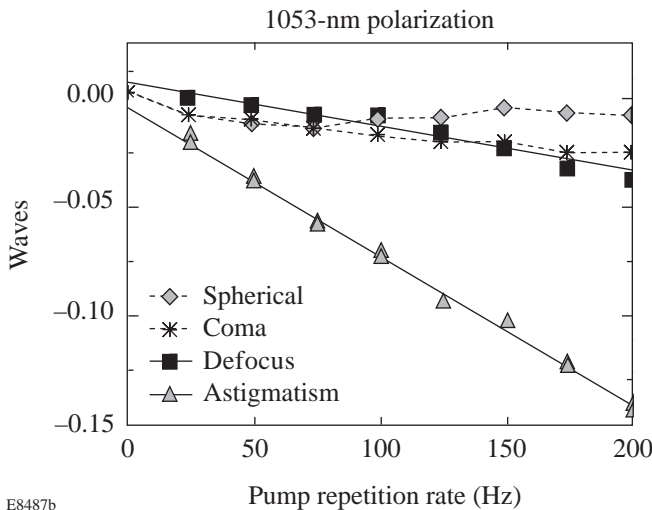
connected by dashed lines. It can be seen from these data that although a small amount of coma and spherical aberration was measured, defocus and astigmatism are the dominant aberrations. Coma and spherical will henceforth be neglected from our analysis. Thermal-focal lengths can be calculated from this data using Eq. (3) with $r_0 = 2.2$ mm (the radius of the rod

aperture used to analyze the fringe data). Figure 71.42 shows the thermally induced dioptric powers (defined as one divided by the thermal-focal length in meters) for the case of the laser-diode-pumped laser rod using π -polarized light in the rod (gain at $\lambda = 1047$ nm), and Fig. 71.43 shows the same data using σ -polarized light in the rod (gain at $\lambda = 1053$ nm). Again the data are fit to straight lines. In these figures, two dioptric powers are given corresponding to the planes parallel and perpendicular to the crystal c axis as described above.



E8487a

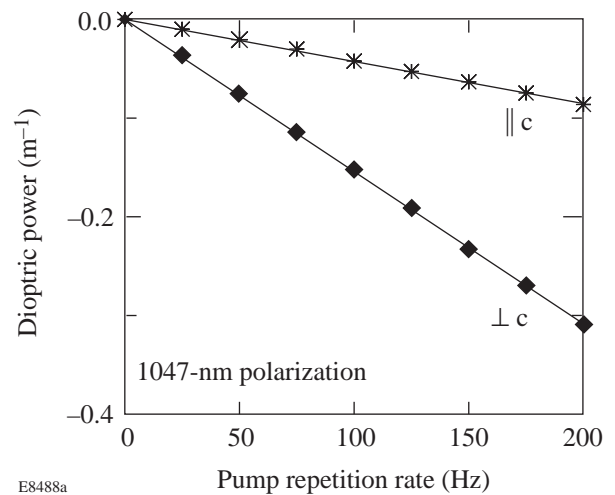
Figure 71.40
Waves of aberration measured with π -polarized light (corresponding to gain at 1047 nm) as a function of the pump repetition rate for our laser-diode-pumped Nd:YLF laser rod pumped to a small-signal gain of 1.8 at 1053 nm.



E8487b

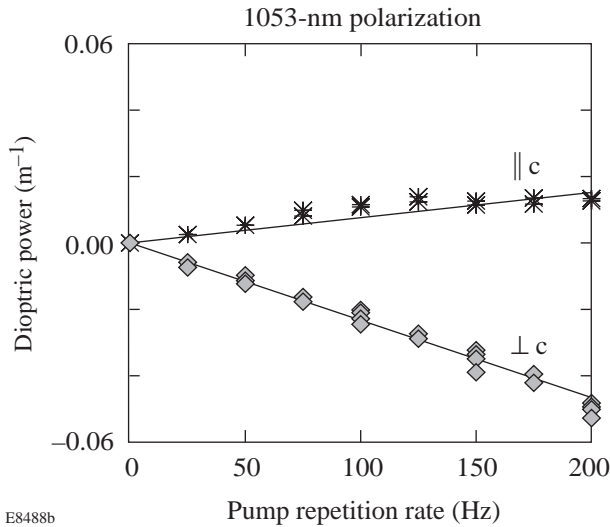
Figure 71.41
Waves of aberration measured with σ -polarized light (corresponding to gain at 1053 nm) as a function of the pump repetition rate for our laser-diode-pumped Nd:YLF laser rod pumped to a small-signal gain of 1.8 at 1053 nm.

For the case of the xenon-flash-lamp-pumped system the thermally induced aberrations using σ -polarized light in the rod (gain at $\lambda = 1053$ nm) were too small to measure since the repetition rate of the flash-lamp power supply was limited to 60 Hz. Figure 71.44 shows the thermally induced dioptric powers (with straight line fits) for the case of the xenon-flash-lamp-pumped laser rod (dashed lines) using π -polarized light in the rod (gain at $\lambda = 1047$ nm). For comparison we have also shown in Fig. 71.44 the same data for the laser-diode-pumped system (taken from Fig. 71.40 and plotted with solid lines). All data in Figs. 71.40–71.44 are taken for the rod pumped to the same small-signal gain (1.8 at 1053 nm). It can be seen that the xenon-flash-lamp-pumped system shows more thermal distortion than the laser-diode-pumped system when pumped to the same small-signal gain.



E8488a

Figure 71.42
Dioptric power (inverse of the thermal-focal length in meters) calculated from the data in Fig. 71.40 as a function of the pump repetition rate. The dioptric power for the plane containing the optic axis (crystal a axis) and the crystal c axis is labeled $\parallel c$ and for the plane containing the optic axis and the crystal b axis is labeled $\perp c$.



E8488b

Figure 71.43

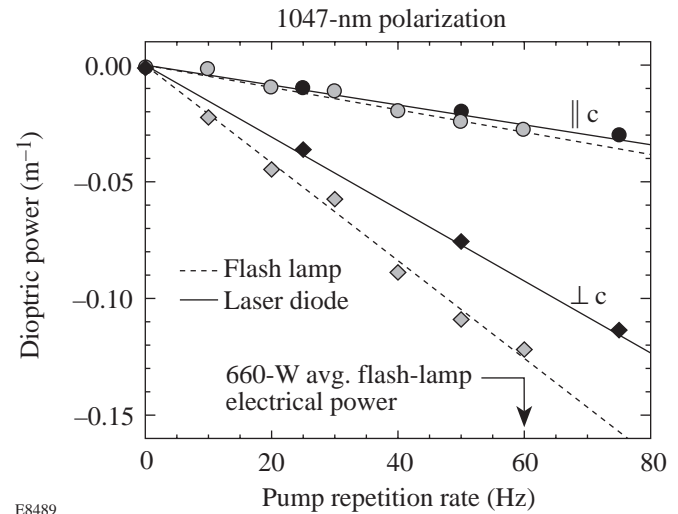
Dioptric power (inverse of the thermal-focal length in meters) calculated from the data in Fig. 71.41 as a function of the pump repetition rate. The dioptric power is labeled $\parallel c$ for the plane containing the optic axis (crystal a axis) and the crystal c axis and $\perp c$ for the plane containing the optic axis and the crystal b axis.

The dioptric powers in Figs. 71.42–71.44 can be written for the two orthogonal planes as¹²

$$D_{\perp,\parallel} = k_{\perp,\parallel} P_a/A, \quad (4)$$

where $D_{\perp,\parallel}$ are the dioptric powers in the planes perpendicular and parallel to the c axis, P_a is the total heat dissipated by the rod (equivalent in steady state to the total heat absorbed by the rod), A is the rod cross-sectional area, and the $k_{\perp,\parallel}$ are the dioptric-power coefficients defined in terms of the material parameters of Nd:YLF.

The heat dissipated by the rod was not measured; however, to compare our dioptric-power measurements to those stated in the literature, we will make similar assumptions: We assume that the total heat dissipated by the rod is proportional to the average electrical power dissipated in the flash lamps, where the proportionality constant involves many coupling efficiencies. We redefine the dioptric-power coefficients in Eq. (4) to include this proportionality constant. We can then calculate these newly defined dioptric-power coefficients using our dioptric-power measurements and the average electrical power dissipated in our xenon flash lamp. When our xenon



E8489

Figure 71.44

Comparison of the dioptric powers (inverse of the thermal-focal length in meters) as a function of the pump repetition rate measured for xenon-flash-lamp-pumped- and laser-diode-pumped Nd:YLF laser rods pumped to the same small-signal gain. The data have been fit to straight lines with the xenon-flash-lamp-pumped data shown as dashed lines and the laser-diode-pumped data (taken from Fig. 71.42) shown as solid lines.

flash lamp is operated at 60 Hz with 11 J per pulse, the average electrical power dissipated in the lamp is 660 W. This calibrates the axes in Figs. 71.42–71.44 to lamp average electrical power, and we can then state dioptric-power coefficients accordingly. Table 71.VII summarizes our dioptric-power coefficients $k_{\perp,\parallel}$, defined in this way, using the appropriate values for the rod areas.

It is coincidental that our dioptric-power measurements for our laser-diode-pumped rod are very similar to those reported by Cerullo *et al.*⁷ for their krypton-flash-lamp-pumped rod. It would be inappropriate, however, to base any conclusions on this since among other things the rods have different diameters and the coupling efficiencies are very different for the two cases. In fact, a true comparison of these data should include a detailed analysis of the cooling and coupling efficiencies mentioned above for each case, since the heat dissipated by the rod is the appropriate quantity to use in Eq. (4). This analysis would go far beyond the intent of this article.

The distortions in the xenon-flash-lamp-pumped rod were also measured at a higher gain. The capacitor-bank voltage was increased from 385 V to 460 V, corresponding to a 43% increase in pump-pulse energy from 11 J per pulse to

Table 71.VII: The coefficients of the thermal-dioptic power as defined in Eq. (4) and discussed in the text.

λ (nm)	Laser diode k_{\parallel} (mm/kW)	Laser diode k_{\perp} (mm/kW)	Xenon flash lamp k_{\parallel} (mm/kW)	Xenon flash lamp k_{\perp} (mm/kW)
1047	-0.767×10^{-3}	-2.76×10^{-3}	-0.565×10^{-3}	-2.38×10^{-3}
1053	-0.566×10^{-3}	$+0.153 \times 10^{-3}$	no data	no data

16 J per pulse. We found that the measured thermal distortions scaled linearly with this corresponding increase in average pump power as expected from Eq. (4). However, if the pump-pulse energy were increased significantly beyond this, the lamp’s spectral output would change and different results would be expected.

The thermal-time constant of the distortions in our laser-diode-pumped rod was measured with the camera and VCR frame sequencer as described above. The data are shown in Fig. 71.45. The thermal distortions were measured using π -polarized light (gain at $\lambda = 1047$ nm) in our laser-diode rod pumped at a 200-Hz repetition rate as in Fig. 71.40. Pumping was removed at time equals zero in Fig. 71.45 (with the cooling liquid left on), and the thermal distortions were measured thereafter at known intervals (determined from the frame sequence numbers of the fringe data). The data points for defocus and astigmatism were fitted to exponential curves

(shown as solid lines in Fig. 71.45), and an exponential decay time constant (time for the aberrations to decay to $1/e$ of their value when pumping was removed) of approximately 1.5 s was obtained. These measurements were also made with the 1053-nm transition, and no significant change in the thermal-time constant could be measured.

Summary

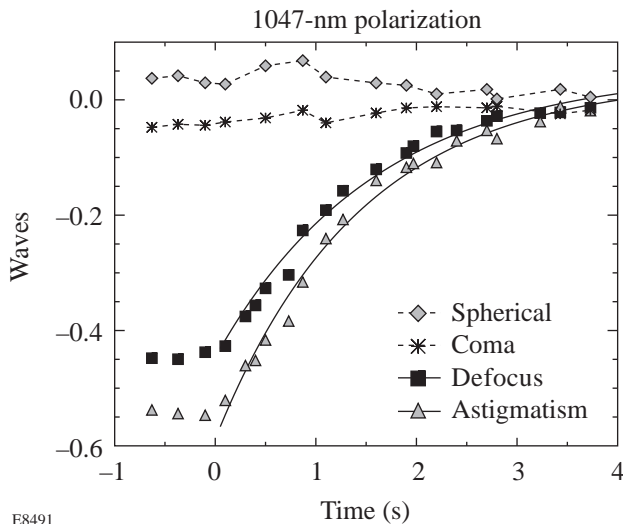
We have made detailed interferometric measurements of the thermal distortions in xenon-flash-lamp- and laser-diode-pumped Nd:YLF laser rods. In both cases, defocus and astigmatism were the dominant thermal distortions. The thermal distortions in our flash-lamp-pumped rod were greater than the thermal distortions in our laser-diode-pumped rod when pumped to the same small-signal gain. Finally, we measured the thermal-relaxation time of our laser-diode-pumped Nd:YLF rod to be approximately 1.5 s.

ACKNOWLEDGMENT

This work was supported by the U.S. Department of Energy Office of Inertial Confinement Fusion under Cooperative Agreement No. DE-FC03-92SF19460, the University of Rochester, and the New York State Energy Research and Development Authority. The support of DOE does not constitute an endorsement by DOE of the views expressed in this article.

REFERENCES

1. Laboratory for Laser Energetics LLE Review **70**, 68, NTIS document No. DOE/SF/19460-164 (1997). Copies may be obtained from the National Technical Information Service, Springfield, VA 22161.
2. J. E. Murray, IEEE J. Quantum Electron. **QE-19**, 488 (1983).
3. H. Vanherzeele, Opt. Lett. **13**, 369 (1988).
4. H. Vanherzeele, Appl. Opt. **27**, 3608 (1988).
5. H. Vanherzeele, Appl. Opt. **28**, 4042 (1989).
6. E. Reed and G. Frangineas, in *Solid State Lasers*, edited by G. Dubé (SPIE, Bellingham, WA, 1990), Vol. 1223, pp. 247–258.
7. G. Cerullo, S. De Silvestri, and V. Magni, Opt. Commun. **93**, 77 (1992).
8. Y. Ichioka and M. Inuiya, Appl. Opt. **11**, 1507 (1972).
9. M. Takeda, H. Ina, and S. Kobayashi, J. Opt. Soc. Am. **72**, 156 (1982).



E8491

Figure 71.45 Thermal relaxation of the aberrations for π -polarized light (corresponding to gain at 1047 nm) in the laser-diode-pumped Nd:YLF laser rod. The rod was operated at 200-Hz pump repetition rate, and pumping was removed at time equals zero. The thermal-relaxation time is 1.5 s.

10. K. H. Womack, *Opt. Eng.* **23**, 391 (1984).
11. L. E. Holder *et al.*, *IEEE J. Quantum Electron.* **28**, 986 (1992).
12. W. Koechner, *Solid-State Laser Engineering*, 3rd ed., Springer Series in Optical Sciences (Springer-Verlag, New York, 1996).
13. M. Born and E. Wolf, *Principles of Optics: Electromagnetic Theory of Propagation, Interference and Diffraction of Light*, 6th ed. (Pergamon Press, Oxford, 1980).